Measurement of Perfusion in Stage IIIA-N2 Non-Small Cell Lung Cancer Using $H_2{}^{15}O$ and Positron Emission Tomography

Corneline J. Hoekstra, Sigrid G. Stroobants, Otto S. Hoekstra, Egbert F. Smit, Johan F. Vansteenkiste, and Adriaan A. Lammertsma[1]

Clinical PET Centre [C. J. H., O. S. H., A. A. L.] and Departments of Pulmonary Medicine [C. J. H., E. F. S.] and Clinical Epidemiology and Biostatistics [O. S. H.], VU University Medical Centre, 1007 MB Amsterdam, the Netherlands, and Departments of Nuclear Medicine [S. G. S.] and Pulmonary Medicine [J. F. V.], University Hospital Gasthuisberg, Leuven, Belgium

ABSTRACT

Purpose: **As the interest in antiangiogenesis therapy in oncology is rising, the need for *in vivo* techniques to monitor such therapy is obvious. Measurement of tumor perfusion using positron emission tomography and $H_2{}^{15}O$ potentially is such a technique. The objective of the present study was to assess whether it is feasible to measure perfusion *in vivo* in non-small cell lung cancer (NSCLC) using $H_2{}^{15}O$ and positron emission tomography.**

Experimental Design: **Fifteen dynamic $H_2{}^{15}O$ and [^{18}F]2-fluoro-2-deoxy-D-glucose (^{18}FDG) studies were performed in 10 patients with stage IIIA-N2 NSCLC. Blood flow (BF) data were correlated with simplified methods of analysis (tumor:normal tissue ratio and standardized uptake value) and with glucose metabolism (MR_{glu}).**

Results: **^{18}FDG data were required for accurate definition of tumor and mediastinal lymph node metastases. There was large intertumor variation in BF. Correlation of simplified methods of analysis with quantitative BF was poor. In addition, BF and MR_{glu} were not correlated.**

Conclusion: **Measurement of BF in NSCLC using $H_2{}^{15}O$ and ^{18}FDG is feasible. Simple uptake analysis, however, cannot be used as an indicator of perfusion. Whether BF can be used for response monitoring needs to be evaluated in a large patient study, where results can be compared with outcome.**

INTRODUCTION

For the development of novel cancer treatment strategies, knowledge of tumor biology is essential. Heterogeneity of tumor perfusion has therapeutic consequences for both drug delivery and distribution and for oxygenation status. If tumor blood flow could be monitored noninvasively, more insight in the efficacy of therapy could be obtained. For example, in a tumor with very poor perfusion, it could be predicted that chemotherapeutics would not reach the tumor and thus not affect it, and other therapy options would have to be considered.

Presently, the interest in inhibition of vascular growth of tumors (antiangiogenesis) as a possible therapeutic strategy increases. Monitoring the effects of angiogenesis inhibitors requires a noninvasive technique to assess the perfusion status of the tumor.

Using PET[2], it is possible to perform physiological measurements *in vivo*. Most oncology studies are performed using ^{18}FDG, which is a tracer of glucose metabolism. However, in those studies where information of the perfusion status of the tumor is needed, water labeled with oxygen-15 ($H_2{}^{15}O$) may be used. Initial PET oncology studies using $H_2{}^{15}O$ were performed in brain tumors (1–7). In tumors outside the central nervous system, only a few studies have been reported (8–19), using a variety of different techniques. To the best of our knowledge, no studies have been reported on the use of $H_2{}^{15}O$ in lung tumors.

The aim of the present study was to develop a method for the measurement of blood flow in lung tumors. After a brief overview of background and theory, initial results of measuring perfusion in stage IIIA-N2 NSCLC patients are presented.

Background. BF can be measured using different tracers and techniques. Of the various tracers, $H_2{}^{15}O$ has the advantage that it is freely diffusible and metabolically inert. In addition, because of the very short half-life of ^{15}O, repeat or combined measurements within a single scanning session can be made. Although several techniques to measure BF using $H_2{}^{15}O$ have been described, they are all based on the original tracer kinetic model proposed by Kety (20).

The steady-state technique, a noninvasive inhalation technique using the steady-state principle, was first described by Jones *et al.* (21) and later implemented for PET by Frackowiak *et al.* (22). In this technique, a static PET scan is performed during continuous inhalation of ^{15}O-labeled carbon dioxide ($C^{15}O_2$). $C^{15}O_2$ is rapidly transferred in the lungs to the water-pool under the influence of carbon anhydrase (23). After an inhalation period of ~10 min and because of the short half-life of ^{15}O, tissue $H_2{}^{15}O$ will reach a dynamic equilibrium in which the diffusion rate from arterial blood into the tissue is balanced by the diffusion rate out of tissue into venous blood and the rate

Received 2/20/01; revised 11/16/01; accepted 11/29/01.
The costs of publication of this article were defrayed in part by the payment of page charges. This article must therefore be hereby marked *advertisement* in accordance with 18 U.S.C. Section 1734 solely to indicate this fact.

[1] To whom requests for reprints should be addressed, at Clinical PET Centre, VU University Medical Centre, P. O. Box 7057, 1007 MB Amsterdam, the Netherlands. Phone: 31-20-4444214; Fax: 31-20-4443090; E-mail: aa.lammertsma@vumc.nl.

[2] The abbreviations used are: PET, positron emission tomography; ^{18}FDG, [^{18}F]2-fluoro-2-deoxy-D-glucose; NSCLC, non-small cell lung cancer; BF, blood flow; SUV, standard uptake value; FBP, filtered back projection; ROI, regions of interest; MLN, mediastinal lymph node; T/N, tumor:normal tissue.

of radioactive decay. The actual scan is started after this equilibration period. Within oncology, the technique has been applied mainly in brain tumor studies (1, 2, 4, 24), in a study in patients with breast carcinoma by Beaney *et al.* (8), and in 2 patients with hepatic tumors by Taniguchi *et al.* (19).

Advantages of the steady-state technique are its simple implementation, even for obtaining functional blood flow images, and the possibility to improve the statistical quality of the data simply by increasing the duration of the scan. An important disadvantage of the steady-state technique is the underestimation of BF in heterogeneous tissue (25, 26). Tumor is known to be nonhomogeneous, being an admixture of clusters of tumor and normal cells, vascular structures, and necrotic tissue. The steady-state technique assumes that the partition coefficient of water equals 1, which might not be valid in tumors (25), and because of the equilibration period prior to scanning, rather inefficient use is made of the administered radiation dose.

As an alternative to the steady-state technique, the so-called autoradiographic method was developed for the first (slow) generation of PET scanners (27–29). In this method, the integral counts over the first period after $H_2{}^{15}O$ injection (*i.e.*, single frame study) are collected. BF is calculated using the measured arterial input function (multiple samples), assuming a fixed partition coefficient of water. The method was validated for the brain using a 40-s integration period after arrival of $H_2{}^{15}O$ in the brain. An advantage over the steady-state method is the much shorter acquisition time, however, at the cost of decreased statistical quality. In addition, there is a more linear relationship between counts and BF than in the steady-state technique. A disadvantage over the steady-state technique is increased sensitivity to the presence of arterial blood. In addition, results were found to be dependent on the integration (acquisition) time, possibly because of delay and dispersion of the arterial input function. The method shares an important disadvantage with the steady-state technique, at least in oncological applications, in that a value for the partition coefficient of water has to be assumed. To the best of our knowledge, the method has not been applied to tumors outside of the brain.

With the introduction of fast multiring PET scanners, dynamic blood flow methods were developed and validated for the brain (30), myocardium (31–34), and tumors (12) outside the central nervous system. Reproducibility in the brain was found to be better than 10% (33). The main advantage of this dynamic technique is that no value for the partition coefficient or volume of distribution of water (V_d) has to be assumed, thereby significantly increasing the accuracy of the BF measurements. In addition, it has been demonstrated that the sensitivity to tissue heterogeneity is low (26), and that the flow estimates are independent of scan duration. Finally, when necessary, it is possible to account for contamination of the tissue signal within arterial blood activity.

To quantify BF an arterial input function is required. The most accurate method to determine this input function is continuous on-line arterial blood sampling. In patients for whom repetitive scans are needed, however, arterial cannulation should, whenever possible, be avoided. For studies of the myocardium and in breast tumor patients, input curves obtained from both the left atrium and left ventricle have been used and validated (34–36).

Table 1 Patient characteristics

	n
Gender	
Male	7
Female	3
Age	
Mean	66.5 years
Range	45–76 years
Histology	
Squamous cell carcinoma	2
Adenocarcinoma	5
Large cell carcinoma	2
Planocellular carcinoma	1
Time scan	
Prior to start chemotherapy	5
After 1 cycle of chemotherapy	6
After 3 cycles of chemotherapy	4

Several studies have been performed using a $H_2{}^{15}O$ bolus injection and PET to assess blood flow in different tumor types (9–16, 18). Some of these studies used the SUV or differential absorption ratio (9, 13, 15, 16, 18) as a measure of tumor BF. Although SUV is used extensively as a measure of glucose metabolism in ^{18}FDG studies, its use is controversial (37). Criticism of the use of SUV would be even more relevant to $H_2{}^{15}O$ studies (*e.g.*, dependence on scan duration and measurement time), and no comparison with measured BF values has been made.

MATERIALS AND METHODS

As part of an ongoing response monitoring study, 15 dynamic $H_2{}^{15}O$ scans were performed in 10 patients using dedicated PET scanners ECAT EXACT HR+ (Siemens/CTI). All patients (7 men, 3 women; mean age, 66.5 years) were clinically staged as having stage IIIA-N2 NSCLC. Patient characteristics are listed in Table 1. The study protocol was approved by the medical ethics committee of both hospitals participating in this study. All patients gave written informed consent.

First, a 10-min transmission scan over the tumor area was performed, followed by injection of $H_2{}^{15}O$ using an automated injector (Med-Rad multilevel CT injector), simultaneously starting a 10-min dynamic emission scan (12 × 5 min, 12 × 10 min, 6 × 20 min, and 10 × 30 min). Injection (1000 MBq dissolved in 2.5 ml) was given as a bolus (15 s; 10 ml/min), followed by a flush of 2 min. Ten min after the $H_2{}^{15}O$ scan (to allow for radioactive decay of ^{15}O), 370 MBq of ^{18}FDG were injected, and a second (60-min) dynamic emission scan with progressive frame lengths was started.

Data Analysis. All dynamic scan data were corrected for dead time, decay, scatter, randoms, and photon attenuation and were reconstructed using FBP with a Hanning filter (cutoff, 0.5 cycles/pixel). This resulted in a transaxial spatial resolution of ~7 mm of full width at half maximum.

ROI were defined automatically over both tumor and MLN metastases by applying a threshold of 50% of the maximum ^{18}FDG pixel value within the lesion. For this purpose, the last three frames (*i.e.*, 45–60 min after injection) of the sinograms of the ^{18}FDG scan were summed and reconstructed using ordered subset expectation maximization with 2 iterations and 12 sub-

sets. This was followed by postsmoothing of the reconstructed image using a 5-mm full width at half maximum Gaussian filter to obtain the same resolution as the dynamic images reconstructed with FBP. The ordered subset expectation maximization reconstructions were used because of their superior image quality, thus facilitating ROI definition. For quantification, however, the more accurate FBP reconstructed images were used (38), and therefore, tumor ROI were copied to the (FBP reconstructed) dynamic $H_2{}^{15}O$ data to create tumor time activity curves. Furthermore, ROI were defined manually over the aortic arch, left ventricle, and left atrium on a summed (FBP) image of the first min of the $H_2{}^{15}O$ scan. These data were used to create an image-derived input function.

Time activity curves were analyzed using standard nonlinear regression techniques and the single compartment model, both with and without an arterial blood volume component (see Appendix, Eqs. C and D, respectively), weighting data for acquired counts and frame duration. In addition, to assess the validity of data presented in the literature, T/N ratios from 0 to 5 min and the SUV corrected for body surface area (SUV_{BSA}) from 0 to 5 and from 4 to 5 min were evaluated.

Glucose consumption (MR_{glu}) was obtained from the ^{18}FDG data using nonlinear regression and the standard two-tissue (3k) compartment model (39) with three rate constants and a blood volume component (40) and an image derived input function (41).

Statistics. The presence of an arterial blood volume component in the tumor curves was assessed by comparing the residual sum of squares with and without such a component using the Akaike (42) and Schwarz (43) criteria. The correlation of T/N and SUV_{BSA} values with both BF and V_d values was assessed, using the Pearson bivariate correlation; $P < 0.01$ was considered to be significant. The correlation of MR_{glu} with BF values was assessed, using Pearson bivariate correlation; again, $P < 0.01$ was considered to be significant.

RESULTS

In Fig. 1, transaxial images at the level of tumor and MLN metastases are shown for both $H_2{}^{15}O$ and ^{18}FDG data. It can be seen that the tumor could have been identified and defined on the $H_2{}^{15}O$ scan itself. However, for the definition of MLN metastases, the ^{18}FDG scan was needed. Therefore, all tissue ROI were defined on the ^{18}FDG scan.

ROI to generate the image-derived input function were defined on summed dynamic $H_2{}^{15}O$ data. For the input function, as many time-activity curves as possible were averaged (weighted to ROI size) to obtain optimal statistics. In 8 scans, the curves from the aortic arch could be used. ROI defined in both the left ventricle and atrium could be used in 13 scans. An example of an average blood time-activity curve (input function) is given in Fig. 2*A*.

Examples of fits with and without an arterial blood volume component are given in Fig. 2*B*. In 14 of 15 scans (93%), incorporating an arterial blood volume component provided significantly better fits according to the Akaike criterion. This was 12 of 15 (80%) according to the Schwarz criterion. Therefore, all results presented here are for the model with arterial blood volume component (*i.e.*, according to Eq. D).

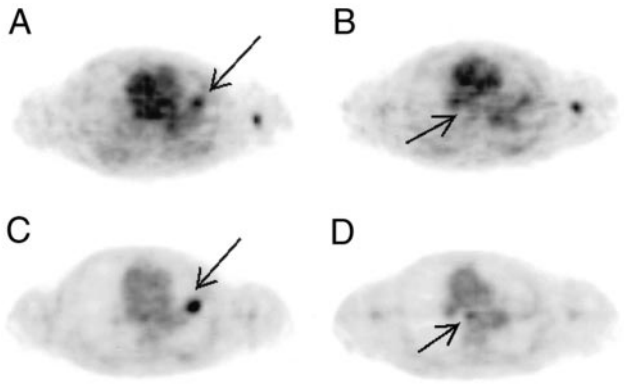

Fig. 1 This figure shows $H_2{}^{15}O$ (*A* and *B*) and ^{18}FDG (*C* and *D*) images for a patient with a left-sided lung tumor and a subcarinal lymph node metastasis. The $H_2{}^{15}O$ images are integral images over the period from 1 to 5 min after injection. The ^{18}FDG images are integrated from 45 to 60 min after injection. Both axial slices at the level of primary tumor (*A* and *C*) and MLN metastasis (*B* and *D*) are shown. The tumor can clearly be seen in the $H_2{}^{15}O$ image; however, the MLN metastasis is difficult to detect based on the $H_2{}^{15}O$ image alone.

Individual values of T/N, SUV_{BSA}, BF, and V_d are presented in Table 2. The mean ± SD for blood flow in tumor was 0.59 ± 0.37 ml/ml/min, with a range of 0.15–1.29 ml/ml/min. For MLN metastases, this was 0.48 ± 0.23 ml/ml/min with a range of 0.21–0.86 ml/ml/min. The mean ± SD value for V_d was 0.63 ± 0.10 with a range of 0.45–0.78 for tumor and 0.74 ± 0.17 with a range of 0.47–0.99 for MLN metastases, respectively.

The correlation between BF and SUV_{BSA} (0–5 min) was 0.60 ($P = 0.02$) and 0.32 ($P = 0.25$) for SUV_{BSA} (4–5 min), which were both not significant. The correlation between BF and T/N ratio was 0.58 ($P = 0.02$). SUV_{BSA} (0–5 min) was also poorly correlated with V_d ($r = 0.49$, $P = 0.06$); for SUV_{BSA} (4–5 min), this was 0.37 ($P = 0.18$).

Values of MR_{glu} are also given in Table 2. The correlation with BF was poor ($r = 0.28$, $P = 0.31$), as illustrated in Fig. 3.

DISCUSSION

Inhibition of angiogenesis in tumors is an important therapeutic aim because it might be a means of preventing progression of disease. Presently, many studies are performed to assess the possibilities of such therapy. It is important to be able to monitor the effects of antiangiogenesis therapy *in vivo*, preferably in a simple and noninvasive manner. A potential means to monitor these effects is the measurement of tumor perfusion. Hence, there is renewed interest in blood flow measurements using PET and $H_2{}^{15}O$.

The most important finding of the present study in lung tumors is the large variation in BF in different tumors, even in the untreated ones. It is likely that this variation has implications for therapy (drug delivery, oxygenation, and others). Therefore, studies are needed to relate perfusion measurements with response to treatment.

In the present study in lung tumors, ROI for tissue time-activity curves and input curves were defined using different datasets. The image-derived input curve was defined using

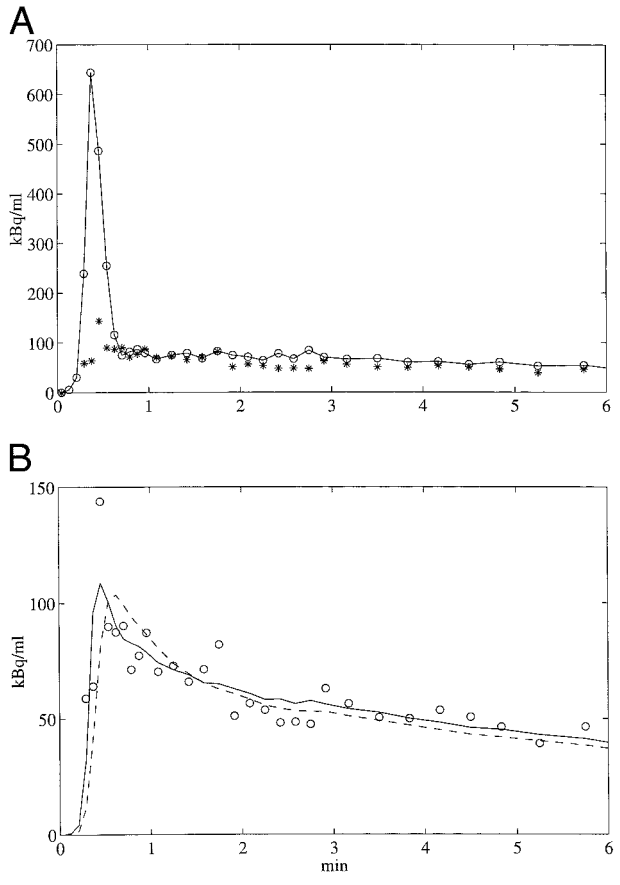

Fig. 2 *A,* example of an average blood time-activity curve (image derived input function). *B,* example of fits of a tumor ROI with (*solid line*) and without (*dashed line*) an arterial blood volume included in the fitting equation. The corresponding input function is given in *A*.

summed (first min) $H_2{}^{15}O$ ROI being defined over the aortic arch, left ventricle, and atrium. The use of the last two has been validated previously for myocardial studies (34). In contrast to ^{18}FDG, only minor spillover effects from the myocardium occur. An input curve derived from the aortic arch has not been described for $H_2{}^{15}O$. When a tumor is located in the apex of the lung, the left ventricle and atrium may not be in the field of view of the scan, resulting in the need for another structure to generate an input function. A disadvantage of the use of the aortic arch is the higher risk of partial volume effects. In the present study in 8 of 15 scans, the input curve from the aortic arch could be used when compared with curves from the left atrium and ventricle. Because $H_2{}^{15}O$ distributes rapidly throughout the body and because of the short half-life of ^{15}O, as many ROI as possible are needed to obtain accurate statistics.

Tissue time-activity curves were defined using the last 15 min of the ^{18}FDG data. Although summing of the first 5 min of the $H_2{}^{15}O$ data provided an acceptable image for the definition of tumor in most patients, the definition of MLN metastases was difficult if not impossible using $H_2{}^{15}O$ data alone (Fig. 1). A disadvantage of the use of tumor ROI defined on ^{18}FDG data are the time gap with the actual $H_2{}^{15}O$ scan, thereby increasing the risk of patient movement and thus inappropriate tumor ROI. However, it was not feasible to consistently define an accurate tumor ROI on $H_2{}^{15}O$ data alone, and for this reason, ^{18}FDG scanning proved to be essential. Very recently, a number of alternative methods for generating parametric images of tumor BF using $H_2{}^{15}O$ have been described (44). In 5 patients with renal cell metastases in the thorax, the lesions could be readily identified in the parametric flow images. Further studies are needed, however, to assess whether those methods would also identify MLN metastases in NSCLC and thus obviate the need for ^{18}FDG in defining ROI. The same applies for parametric methods, which thus far have only been applied to the brain (45–48) or heart (49). In theory, ROI could also be defined on CT scans. This, however, would require accurate positioning and realignment between CT and PET scans. In practice, this is not possible because patient positioning routinely is different for CT (hands up) and PET (hands down).

In the model used, it is assumed that water is freely diffusible, *i.e.*, that the extraction fraction is 100%. This is likely to be the case for low flow values. For high flow values, however, extraction could be $<$100%, resulting in an underestimation of flow. This effect is expected to be small because blood vessels supplying a tumor are usually more permeable than normal blood vessels.

In studies performed in brain, the mean volume of distribution of water was found to be 0.86 with a SD of 0.04 (50). For comparison, the mean value of V_d found in breast tumors was 0.56 with a SD of 0.15 (12). In this study, a mean value of 0.63 for NSCLC was found (Table 2), which is very similar to the value found in breast tumors. It should be noted that the estimation of V_d is susceptible to tissue heterogeneity. For example, in the brain the underestimation attributable to tissue heterogeneity can be as high as 30% (26). In contrast, in the same study, the effect of tissue heterogeneity on flow was $<$5% (26).

An arterial blood volume component significantly contributing to the counts within the tumor ROI was present in 80–93% of the scans in this study. In addition, for MLN metastases this was 100%. In brain and breast cancer studies (12, 30, 33), the contribution of an arterial blood volume component was found to be negligible. However, in NSCLC, the contribution needs to be taken into account (see, for example, Fig. 2*B*).

In this study, there was no significant correlation between BF and SUV or T/N ratio. Although the study was limited to a single tumor type, it is likely that the same applies to other tumors. In other words, unless validated for the tumor under investigation, both SUV and T/N ratios cannot be used as indicators of tumor perfusion.

When comparing MR_{glu} with BF, a poor correlation was found (Fig. 3). This would indicate that perfusion and glucose consumption are not coupled in NSCLC, and therefore, as expected, $H_2{}^{15}O$ and ^{18}FDG provide complimentary information on tumor physiology. Whether BF alone, or in combination with ^{18}FDG, may predict response to therapy will have to be investigated in a larger patient study where results can be compared with outcome.

In conclusion, although the uptake of $H_2{}^{15}O$ in NSCLC is higher than in normal lung tissue (T/N $>$1), it is difficult to determine the exact location. This is especially true for possible MLN metastases because of their position close to vascular structures with high tracer concentration. Therefore at present,

Table 2 Patient Data

Patient	Time of scanning	Age	Histology tumor	T/N (0–5 min)	SUV_{bsa} (4–5 min)	SUV_{bsa} (0–5 min)	BF (ml/ml/min)	V_d	MR_{glu} (micromol/ml/min)
1	Prior to start chemotherapy	67	Large cell carcinoma	2	95	112	0.53	0.62	0.119
2	Prior to start second cycle chemotherapy	76	Planocellular carcinoma	2.7	82	111	1.16	0.78	0.169
3a	Prior to start chemotherapy	70	Adenocarcinoma	5	106	127	0.95	0.76	0.210
3b	Prior to start second cycle chemotherapy			2.5	91	104	0.77	0.69	0.141
4	Prior to start chemotherapy	66	Adenocarcinoma	1.6	80	69	0.19	0.71	0.165
5	Prior to start second cycle chemotherapy	76	Large cell carcinoma	2.2	70	76	0.25	0.65	0.122
6	Prior to start second cycle chemotherapy	62	Adenocarcinoma	3.9	85	100	0.90	0.74	0.097
7a	Prior to start chemotherapy	62	Adenocarcinoma	2.4	71	89	0.53	0.68	0.137
7b	Prior to start second cycle chemotherapy			2.2	55	75	1.29	0.52	0.090
7c	Prior to start third (last) cycle chemotherapy			1.8	63	85	0.50	0.55	0.054
8a	Prior to start chemotherapy	74	Squamous cell carcinoma	1.7	80	74	0.43	0.63	0.235
8b	Prior to start second cycle chemotherapy			1.9	59	65	0.15	0.61	0.070
8c	Prior to start third (last) cycle chemotherapy			1.3	53	53	0.22	0.45	0.071
9	Prior to start third (last) cycle chemotherapy	68	Squamous cell carcinoma	1.4	55	59	0.21	0.48	0.035
10	Prior to start chemotherapy		Adenocarcinoma	1.8	144	141	0.73	0.56	0.170

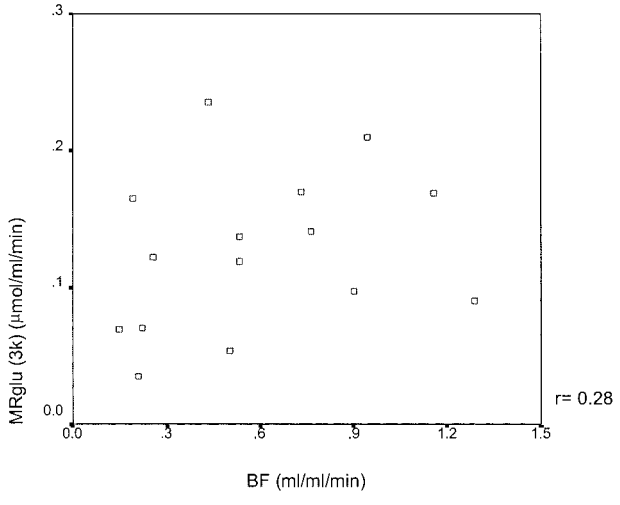

Fig. 3 Scatter diagram of MR_{glu} *versus* BF, illustrating poor correlation ($r = 0.28$, $P = 0.31$).

the study needs to be combined with, for example, an ^{18}FDG study for accurate ROI definition.

When performing dynamic blood flow PET using $H_2{}^{15}O$ in NSCLC, the influence of an arterial blood volume component has to be taken into account. The volume of distribution of water is similar to reported values for breast tumors.

An important finding is the large intertumor variation in perfusion. This could indicate that perfusion might be an important parameter for predicting therapy efficacy. The actual additional value of PET using $H_2{}^{15}O$ for monitoring antiangiogenesis therapy needs to be evaluated further in a larger serial patient study. In addition, the value of combining $H_2{}^{15}O$ and ^{18}FDG studies will need further investigation.

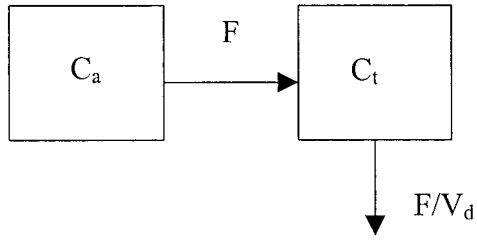

Fig. 4 Schematic diagram of the single tissue compartment model. For a full description, see the main text.

APPENDIX

For the present study, flow was measured using the dynamic method based on the tracer kinetic model originally described by Kety (20, 51). The single tissue compartment model is illustrated in Fig. 4, where it is assumed that all concentrations are corrected for decay. The rate of change of activity in tissue is the balance between delivery and washout, or in mathematical terms:

$$dC_t/dt = FC_a - (F/V_d) \cdot Ct \quad (A)$$

where F is BF or perfusion (ml blood/ml tissue/min), V_d is the partition coefficient or volume of distribution of water (unitless), C_a is the concentration of $H_2{}^{15}O$ in arterial blood (kBq/ml), and C_t is the concentration of $H_2{}^{15}O$ in tissue (kBq/ml).

The solution of this differential equation is:

$$C_t = F \cdot C_a \otimes e^{-F/Vd \cdot t} \quad \text{(B)}$$

where $\otimes$ represents the operation of convolution.

The method is based on the following assumptions: (*a*) flow (F) and V_d are constant during the period of measurement, *i.e.*, the system is in a physiological steady state; (*b*) $H_2{}^{15}O$ is a freely diffusible tracer, *i.e.*, the extraction fraction of water is unity, and no binding of water in tissue occurs; (*c*) $H_2{}^{15}O$ that diffuses into tissue equilibrates instantaneously within the tissue, *i.e.*, there are no concentration gradients in tissue; (*d*) venous and tissue concentrations do not differ, *i.e.*, the volume of distribution (V_d), or the partition coefficient, is close to 1. This means that the venous blood can be considered to be at tissue concentration and, therefore, venous blood and tissue can be considered to be a single compartment; and (*e*) the contribution of arterial blood activity, *i.e.*, the signal arising from arterial activity within a ROI is negligible.

The last assumption states that tissue and (measured) ROI concentration are the same, *i.e.*:

$$C_{ROI} = C_t \quad \text{(C)}$$

where C_t is given by Eq. B.

If the signal arising from the arterial blood is not negligible, this can be accounted for by incorporating an additional arterial blood volume (V_a) term resulting in:

$$C_{ROI} = (1 - V_a)\, C_t + V_a C_a \quad \text{(D)}$$

REFERENCES

1. Ito, M., Lammertsma, A. A., Wise, R. J., Bernardi, S., Frackowiak, R. S., Heather, J. D., McKenzie, C. G., Thomas, D. G., and Jones, T. Measurement of regional cerebral blood flow and oxygen utilisation in patients with cerebral tumours using ^{15}O and positron emission tomography: analytical techniques and preliminary results. Neuroradiology, *23:* 63–74, 1982.

2. Lammertsma, A. A., Wise, R. J., and Jones, T. *In vivo* measurements of regional cerebral blood flow and blood volume in patients with brain tumours using positron emission tomography. Acta Neurochir., *69:* 5–13, 1983.

3. Beaney, R. P., Brooks, D. J., Leenders, K. L., Thomas, D. G., Jones, T., and Halnan, K. E. Blood flow and oxygen utilisation in the contralateral cerebral cortex of patients with untreated intracranial tumours as studied by positron emission tomography, with observations on the effect of decompressive surgery. J. Neurol. Neurosurg. Psychiatry, *48:* 310–319, 1985.

4. Lammertsma, A. A., Wise, R. J., Cox, T. C., Thomas, D. G., and Jones, T. Measurement of blood flow, oxygen utilisation, oxygen extraction ratio, and fractional blood volume in human brain tumours and surrounding oedematous tissue. Br. J. Radiol., *58:* 725–734, 1985.

5. Mineura, K., Yasuda, T., Kowada, M., Shishido, F., Ogawa, T., and Uemura, K. Quantitative analysis of regional cerebral hemodynamics and metabolism in gliomas using O-15 and F-18-fluorodeoxyglucose (FDG) PET. Proceedings of the International Symposium on Current and Future Aspects of Cancer Diagnosis with Positron Emission Tomography, pp. 82–85. Senda, Japan, 1985.

6. Taki, W., Handa, H., Ishikawa, M., Kobayashi, A., Yamashita, J., Yonekawa, Y., Tanada, S., Senda, M., Yonekura, Y., Torizuka, K., Fujita, T., Fukuyama, H., Fukimota, N., Harada, K., and Kameyama, M. Blood flow and oxygen utilization in brain tumors. Proceedings of the International Symposium on Current and Future Aspects of Cancer Diagnosis with Positron Emission Tomography. Tohoku University, 91–95, 1985.

7. Mineura, K., Yasuda, T., Kowada, M., Shishido, F., Ogawa, T., and Uemura, K. Positron emission tomographic evaluation of histological malignancy in gliomas using oxygen-15 and fluorine-18-fluorodeoxyglucose. Neurol. Res., *8:* 164–168, 1986.

8. Beaney, R. P., Lammertsma, A. A., Jones, T., McKenzie, C. G., and Halnan, K. E. Positron emission tomography for *in-vivo* measurement of regional blood flow, oxygen utilisation, and blood volume in patients with breast carcinoma. Lancet, *1:* 131–134, 1984.

9. Strauss, L. G., Clorius, J. H., Schlag, P., Lehner, B., Kimmig, B., Engenhart, R., Marin-Grez, M., Helus, F., Oberdorfer, F., and Schmidlin, P. Recurrence of colorectal tumors: PET evaluation. Radiology, *170:* 329–332, 1989.

10. Kubo, S., Yamamoto, K., Magata, Y., Iwasaki, Y., Tamaki, N., Yonekura, Y., and Konishi, J. Assessment of pancreatic blood flow with positron emission tomography and oxygen-15 water. Ann. Nucl. Med., *5:* 133–138, 1991.

11. Wilson, C. B., Snook, D. E., Dhokia, B., Taylor, C. V., Watson, I. A., Lammertsma, A. A., Lambrecht, R., Waxman, J., Jones, T., and Epenetos, A. A. Quantitative measurement of monoclonal antibody distribution and blood flow using positron emission tomography and ^{124}iodine in patients with breast cancer. Int. J. Cancer, *47:* 344–347, 1991.

12. Wilson, C. B., Lammertsma, A. A., McKenzie, C. G., Sikora, K., and Jones, T. Measurements of blood flow and exchanging water space in breast tumors using positron emission tomography: a rapid and noninvasive dynamic method. Cancer Res., *52:* 1592–1597, 1992.

13. Dimitrakopoulou-Strauss, A., Strauss, L. S., Goldschmidt, H., Lorenz, W. J., Maier-Borst, W., and van Kaick, G. Evaluation of tumour metabolism and multidrug resistance in patients with treated malignant lymphomas. Eur. J. Nucl. Med., *22:* 434–442, 1995.

14. Ziegler, S. I., Haberkorn, U., Byrne, H., Tong, C., Kaja, S., Richolt, J. A., Schosser, R., Krieter, H., Lammertsma, A. A., and Price, P. Measurement of liver blood flow using oxygen-15 labelled water and dynamic positron emission tomography: limitations of model description. Eur. J. Nucl. Med., *23:* 169–177, 1996.

15. Kuhn, G., Reiser, C., Dimitrakopoulou-Strauss, A., Oberdorfer, F., and Strauss, L. G. PET studies of perfusion and glucose metabolism in patients with untreated head and neck tumours. Onkologie, *20:* 226–230, 1997.

16. Dimitrakopoulou-Strauss, A., Strauss, L. G., Schlag, P., Hohenberger, P., Irngartinger, G., Oberdorfer, F., Doll, J., and van Kaick, G. Intravenous and intra-arterial oxygen-15-labeled water and fluorine-18-labeled fluorouracil in patients with liver metastases from colorectal carcinoma. J. Nucl. Med., *39:* 465–473, 1998.

17. Ponto, L. L. B., Madsen, M. T., Hichwa, R. D., Mayr, N., Yuh, W. T. C., Magnotta, V. A., Watkins, G. L., and Ehrhardt, J. C. Assessment of blood flow in solid tumors using PET. Clin. Positron Imaging, *1:* 117–121, 1998.

18. Schwarzbach, M., Willeke, F., Dimitrakopoulou-Strauss, A., Strauss, L. G., Zhang, Y. M., Mechtersheimer, G., Hinz, U., Lehnert, T., and Herfarth, C. Functional imaging and detection of local recurrence in soft tissue sarcomas by positron emission tomography. Anticancer Res., *19:* 1343–1349, 1999.

19. Taniguchi, H., Yamaguchi, A., Kunishima, S., Koh, T., Masuyama, M., Koyama, H., Oguro, A., and Yamagishi, H. Using the spleen for time-delay correction of the input function in measuring hepatic blood flow with oxygen-15 water by dynamic PET. Ann. Nucl. Med., *13:* 215–221, 1999.

20. Kety, S. The theory and application of the exchange of inert gas at the lungs and tissues. Pharmacol. Rev., *3:* 1–41, 1951.

21. Jones, T., Chesler, D. A., and Ter Pogossian, M. M. The continuous inhalation of oxygen-15 for assessing regional oxygen extraction in the brain of man. Br. J. Radiol., *49:* 339–343, 1976.

22. Frackowiak, R. S., Lenzi, G. L., Jones, T., and Heather, J. D. Quantitative measurement of regional cerebral blood flow and oxygen metabolism in man using ^{15}O and positron emission tomography: theory, procedure, and normal values. J. Comput. Assist. Tomogr., *4:* 727–736, 1980.

23. West, J. B., and Dollery, C. T. Uptake of oxygen-15 labeled CO_2 compared with carbon-11 labeled CO_2 in the lung. J. Appl. Physiol., *17:* 9–13, 1962.

24. Brooks, D. J., Beaney, R. P., Thomas, D. G., Marshall, J., and Jones, T. Studies on regional cerebral pH in patients with cerebral tumours using continuous inhalation of $^{11}CO_2$ and positron emission tomography. J. Cereb. Blood Flow Metab., *6:* 529–535, 1986.

25. Lammertsma, A. A., and Jones, T. Low oxygen extraction fraction in tumours measured with the oxygen-15 steady state technique: effect of tissue heterogeneity. Br. J. Radiol., *65:* 697–700, 1992.

26. Blomqvist, G., Lammertsma, A. A., Mazoyer, B., and Wienhard, K. Effect of tissue heterogeneity on quantification in positron emission tomography. Eur. J. Nucl. Med., *22:* 652–663, 1995.

27. Ginsberg, M. D., Lockwood, A. H., Busto, R., Finn, R. D., Butler, C. M., Cendan, I. E., and Goddard, J. A simplified *in vivo* autoradiographic strategy for the determination of regional cerebral blood flow by positron emission tomography: theoretical considerations and validation studies in the rat. J. Cereb. Blood Flow Metab., *2:* 89–98, 1982.

28. Herscovitch, P., Markham, J., and Raichle, M. E. Brain blood flow measured with intravenous $H_2{}^{15}O$. I. Theory and error analysis. J. Nucl. Med., *24:* 782–789, 1983.

29. Raichle, M. E., Martin, W. R., Herscovitch, P., Mintun, M. A., and Markham, J. Brain blood flow measured with intravenous $H_2{}^{15}O$. II. Implementation and validation. J. Nucl. Med., *24:* 790–798, 1983.

30. Lammertsma, A. A., Frackowiak, R. S., Hoffman, J. M., Huang, S. C., Weinberg, I. N., Dahlbom, M., MacDonald, N. S., Hoffman, E. J., Mazziotta, J. C., and Heather, J. D. The $C_{15}O_2$ build-up technique to measure regional cerebral blood flow and volume of distribution of water. J. Cereb. Blood Flow Metab., *9:* 461–470, 1989.

31. Iida, H., Kanno, I., Takahashi, A., Miura, S., Murakami, M., Takahashi, K., Ono, Y., Shishido, F., Inugami, A., and Tomura, N. Measurement of absolute myocardial blood flow with $H_2{}^{15}O$ and dynamic positron-emission tomography. Strategy for quantification in relation to the partial-volume effect. Circulation, *78:* 104–115, 1988.

32. Bergmann, S. R., Herrero, P., Markham, J., Weinheimer, C. J., and Walsh, M. N. Noninvasive quantitation of myocardial blood flow in human subjects with oxygen-15-labeled water and positron emission tomography. J. Am. Coll. Cardiol., *14:* 639–652, 1989.

33. Lammertsma, A. A., Cunningham, V. J., Deiber, M. P., Heather, J. D., Bloomfield, P. M., Nutt, J., Frackowiak, R. S., and Jones, T. Combination of dynamic and integral methods for generating reproducible functional CBF images. J. Cereb. Blood Flow Metab., *10:* 675–686, 1990.

34. Araujo, L. I., Lammertsma, A. A., Rhodes, C. G., McFalls, E. O., Iida, H., Rechavia, E., Galassi, A., De Silva, R., Jones, T., and Maseri, A. Noninvasive quantification of regional myocardial blood flow in coronary artery disease with oxygen-15-labeled carbon dioxide inhalation and positron emission tomography. Circulation, *83:* 875–885, 1991.

35. Weinberg, I. N., Huang, S. C., Hoffman, E. J., Araujo, L., Nienaber, C., Grover-McKay, M., Dahlbom, M., and Schelbert, H. Validation of PET-acquired input functions for cardiac studies. J. Nucl. Med., *29:* 241–247, 1988.

36. Iida, H., Rhodes, C. G., De Silva, R., Araujo, L. I., Bloomfield, P. M., Lammertsma, A. A., and Jones, T. Use of the left ventricular time-activity curve as a noninvasive input function in dynamic oxygen-15-water positron emission tomography. J. Nucl. Med., *33:* 1669–1677, 1992.

37. Keyes, J. W. J. SUV: standard uptake or silly useless value? J Nucl. Med., *36:* 1836–1839, 1995.

38. Boellaard, R., van Lingen, A., and Lammertsma, A. A. Experimental and clinical evaluation of iterative reconstruction (OSEM) in dynamic PET: quantitative characteristics and effects on kinetic modeling. J. Nucl. Med., *42:* 808–817, 2001.

39. Phelps, M. E., Huang, S. C., Hoffman, E. J., Selin, C., Sokoloff, L., and Kuhl, D. E. Tomographic measurement of local cerebral glucose metabolic rate in humans with (F-18)2-fluoro-2-deoxy-D-glucose: validation of method. Ann. Neurol., *6:* 371–388, 1979.

40. Hoekstra, C., Paglianiti, I., Hoekstra, O., Smit, E. F., Postmus, P. E., Teule, G. J. J., and Lammertsma, A. A. Monitoring response to therapy in cancer using [18F]-2-fluoro-2-deoxy-D-glucose and positron emission tomography: an overview of different analytical methods. Eur. J. Nucl. Med., *27:* 731–743, 2000.

41. Hoekstra, C., Hoekstra, O., and Lammertsma, A. A. On the use of image derived input functions in oncological FDG PET studies. Eur. J. Nucl. Med., *26:* 1489–1492, 1999.

42. Akaike, H. A new look at the statistical identification. IEEE Trans. Automat. Contr., *19:* 716–723, 1978.

43. Schwarz, G. Estimating the dimension of a model. Ann. Stat., *6:* 461–464, 1978.

44. Lodge, M. A., Carson, R. E., Carrasquillo, J. A., Whatley, M., Libutti, S. K., and Bacharach, S. L. Parametric images of blood flow in oncology PET studies using [^{15}O]water. J. Nucl. Med., *41:* 1784–1792, 2000.

45. Huang, S. C., Carson, R. E., Hoffman, E. J., Carson, J., MacDonald, N., Barrio, J. R., and Phelps, M. E. Quantitative measurement of local cerebral blood flow in humans by positron computed tomography and ^{15}O-water. J. Cereb. Blood Flow Metab., *3:* 141–153, 1983.

46. Alpert, N. M., Eriksson, L., Chang, J. Y., Bergstrom, M., Litton, J. E., Correia, J. A., Bohm, C., Ackerman, R. H., and Taveras, J. M. Strategy for the measurement of regional cerebral blood flow using short-lived tracers and emission tomography. J. Cereb. Blood Flow Metab., *4:* 28–34, 1984.

47. Koeppe, R. A., Holden, J. E., and Ip, W. R. Performance comparison of parameter estimation techniques for the quantitation of local cerebral blood flow by dynamic positron computed tomography. J. Cereb. Blood Flow Metab., *5:* 224–234, 1985.

48. Carson, R. E., Huang, S. C., and Green, M. V. Weighted integration method for local cerebral blood flow measurements with positron emission tomography. J. Cereb. Blood Flow Metab., *6:* 245–258, 1986.

49. Hermansen, F., Ashburner, J., Spinks, T. J., Kooner, J. S., Camici, P. G., and Lammertsma, A. A. Generation of myocardial factor images directly from the dynamic oxygen-15-water scan without use of an oxygen-15-carbon monoxide blood-pool scan. J. Nucl. Med., *39:* 1696–1702, 1998.

50. Lammertsma, A. A., Martin, A. J., Friston, K. J., and Jones, T. *In vivo* measurement of the volume of distribution of water in cerebral grey matter: effects on the calculation of regional cerebral blood flow. J. Cereb. Blood Flow Metab., *12:* 291–295, 1992.

51. Kety, S. Measurement of local blood flow by the exchange of an inert, diffusable substance. Methods Med. Res., *8:* 228–236, 1960.